

# Quantum phase diagram of the spin- $\frac{1}{2}$ Heisenberg antiferromagnet on the square-kagome lattice: a tensor network study

Saeed S. Jahromi<sup>1,2,\*</sup> and Yasir Iqbal<sup>2,†</sup>

<sup>1</sup>*Department of Physics, Institute for Advanced Studies in Basic Sciences (IASBS), Zanjan 45137-66731, Iran*

<sup>2</sup>*Department of Physics and Quantum Centre of Excellence for Diamond and Emergent Materials (QuCenDiEM), Indian Institute of Technology Madras, Chennai 600036, India*

We assess the quantum phase diagram of the spin- $\frac{1}{2}$  Heisenberg antiferromagnetic model on the square-kagome lattice upon varying the two symmetry inequivalent nearest-neighbor couplings,  $J_1$  on squares and  $J$  on triangles. Employing large-scale tensor network simulations based on infinite projected entangled pair states, we find four distinct valence bond crystal (VBC) states and a ferrimagnetically ordered region. Starting from the limit of weakly interacting squares for small  $J/J_1$  where a plaquette cross-dimer VBC with long-range singlets is stabilized, we show that with increasing  $J/J_1$  it transitions to a VBC with resonances over hexagons, the so-called loop-six VBC, which persists across the isotropic point. Interestingly, a generalized version of the pinwheel VBC, earlier reported to be a closely competing state for the isotropic model is energetically stabilized in a sliver of parameter space right beyond the isotropic point. For further increases in  $J/J_1$ , a decorated loop-six VBC occupies an appreciable region of parameter space before transitioning into an imperfect ferrimagnet which finally evolves into a Lieb ferrimagnet. Our characterization of the underlying phases and phase transitions is based on a careful analysis of the energy, magnetization, spin-spin correlations, and bond entanglement entropy.

*Introduction.* Geometric frustration underpins the emergence of novel quantum phases of matter, which includes a large class of quantum paramagnets such as quantum spin liquids [1, 2] described within the resonating valence bond paradigm [3, 4] and valence bond crystals (VBCs) [2]. Of particular interest are lattices composed of a corner-sharing arrangement of triangles, since here, antiferromagnetic Heisenberg interactions between spins conspire with geometric frustration to induce a non-trivial infinite degeneracy of classical ground states [5–8]. In such scenarios, quantum fluctuations at  $T = 0$  often fail to lift this degeneracy giving rise to strongly correlated nonmagnetic phases. Indeed, on the celebrated kagome lattice, the spin  $S = 1/2$  Heisenberg antiferromagnet represents a classic problem [9–15], having been the focal point of rigorous theoretical and experimental investigations [16] aimed at characterizing the true nature of its ground state, which according to the latest state-of-the-art numerical approaches, is believed to be a  $U(1)$  Dirac spin liquid [17–21].

The quest for theoretical and experimental realization of QSLs has recently garnered considerable attention towards quantum magnets exhibiting a novel kagome-like structure referred to as the shuriken or square-kagome lattice [22] [see Fig. 1]. It is a four coordinated lattice formed by corner-sharing triangles with two symmetry-inequivalent nearest-neighbor bonds, and two sets of symmetry-inequivalent sites which makes it a non-Archimedean lattice. The field of quantum materials is now poised with the arrival of new compounds such as  $\text{KCu}_6\text{AlBiO}_4(\text{SO}_4)_5\text{Cl}$  [23, 24],  $\text{KCu}_7\text{TeO}_4(\text{SO}_4)_5\text{Cl}$  [25],  $\text{Na}_6\text{Cu}_7\text{BiO}_4(\text{PO}_4)_4[\text{Cl},(\text{OH})]_3$  [26, 27] and  $\text{ACu}_7\text{TeO}_4(\text{SO}_4)_5\text{Cl}$  ( $A=\text{Na}, \text{K}, \text{Rb}, \text{Cs}$ ) [28, 29], where the  $S = 1/2$   $\text{Cu}^{2+}$  ions form essentially decoupled layers of square-kagome lattices. Most interestingly, recent experimental observations suggest that some of these compounds exhibit no sign of magnetic ordering down to 50

mK with indications for the formation of a gapless quantum spin liquid in  $\text{KCu}_6\text{AlBiO}_4(\text{SO}_4)_5\text{Cl}$  [23], quantum paramagnet in  $\text{Na}_6\text{Cu}_7\text{BiO}_4(\text{PO}_4)_4[\text{Cl},(\text{OH})]_3$  [26, 27, 30] and  $\text{RbCu}_7\text{TeO}_4(\text{SO}_4)_5\text{Cl}$  [28], and a field induced quantum spin liquid in  $\text{KCu}_7\text{TeO}_4(\text{SO}_4)_5\text{Cl}$  [25, 31]. Furthermore, theoretical investigations of the  $S = 1/2$  Heisenberg antiferromagnetic model, Eq. (1), with bond anisotropic exchange interactions ( $J_1, J_2, J_3$ ) [see Fig. 1(a)] on the square-kagome lattice suggest that the ground state phase diagram has the potential to accommodate a variety of nonmagnetic phases [32], including topological spin liquids (possibly nematic) [33], VBCs [34–36], and commensurate as well as incommensurate orders [33]. However, given the limited scope of theoretical approaches employed thus far, there is no consensus regarding the nature and extent of the phases and associate phase transitions, especially in the intermediate coupling regime which is theoretically most challenging, and the quantum phase diagram remains *terra incognita*.

Thus, motivated by the theoretical scope of the model in realization of exotic nonmagnetic phases and its possible experimental relevance, we investigate the  $S = 1/2$  Heisenberg AFM model on the square-kagome lattice along the isotropic line  $J_2 = J_3 \equiv J$ . The  $J_1$ - $J$  phase diagram is mapped using large-scale tensor-network (TN) [37–39] simulations based on infinite projected entangled-pair states (iPEPS) Ansatz [40–42] which allows us to accurately incorporate the subtle interplay between long-range entanglement and short-distance energetics which has been argued to be crucial in reliably ascertaining the precise nature of the quantum phases [36]. This is achieved via an accurate estimation of the ground state energy together with a careful analysis of the magnetization and spin-spin correlations, as well as entanglement entropy. In addition to the previously observed ferrimagnetic state that emerges in the  $J/J_1 \gg 1$  regime, we reveal a rich variety of VBC orders within the intermediate coupling regime which are distinguished by distinct symmetry of strong and weak bond correlation patterns.

*Model and Method.* The nearest-neighbor antiferromag-

\* saeed.jahromi@iasbs.ac.ir

† yiqbal@physics.iitm.ac.in

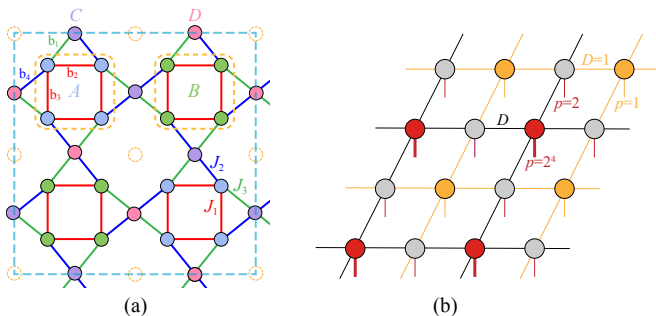


FIG. 1. (a) The translation invariant unit cell of the square-kagome lattice with 24 sites. The blue and green sites represent the two effective sublattices,  $A$  and  $B$ , formed by squares. The purple and pink vertices further represent another set of sublattices,  $C$  and  $D$ , formed by triangles. (b) The corresponding coarse-grained iPEPS tensor networks with square geometry.

netic Heisenberg model on the square-kagome lattice is

$$\hat{\mathcal{H}} = J_1 \sum_{\langle ij \rangle} \hat{\mathbf{S}}_i \cdot \hat{\mathbf{S}}_j + J \sum_{\langle ij \rangle} \hat{\mathbf{S}}_i \cdot \hat{\mathbf{S}}_j, \quad (1)$$

where,  $\hat{\mathbf{S}}_i$  are  $S = 1/2$  operators, and the sum runs over nearest-neighbor links of the lattice. While the generic model involves three distinct couplings as illustrated in Fig. 1(a), here, we fix  $J_2 = J_3 \equiv J$ . We set  $J_1 = 1$  as the energy scale and explore the phase diagram as a function of  $J$  within the range  $0 \leq J \leq 2$ .

In order to simulate the  $S = 1/2$  antiferromagnetic Heisenberg (AFH) model on the square-kagome lattice, we employ the infinite version of the iPEPS algorithm [40–42], specifically adapted for infinite square lattices. In addition, to obtain the tensor network representation of the wave function, we utilized the simple-update algorithm [43] equipped with second-order Suzuki-Trotter decomposition for the evolution operators. To approximate the complete contraction of the 2D iPEPS tensor network for the computation of variational energies and expectation values, the corner transfer-matrix renormalization group method is used [40, 44].

To adapt the iPEPS algorithm designed for square lattices directly to the square-kagome structure and approximate its ground state wave function with a square iPEPS tensor network, we initially coarse-grain the square-kagome lattice [36, 45]. This involves associating a local PEPS tensor with a physical dimension of  $p = 2^4$ , representing the four spins within a square plaquette of the square-kagome lattice [depicted as red tensors in Fig. 1(b)]. Subsequently, we assign a distinct PEPS tensor with a physical dimension of  $p = 2$  to the remaining sites located at the vertices of the triangles [depicted as gray tensors in Fig. 1(b)]. Finally, to achieve a fully translation invariant iPEPS network with a square geometry, we introduce dummy tensors with trivial physical and virtual indices at the center of each octagon [represented by yellow tensors in Fig. 1(b)]. The original square-kagome lattice and its corresponding TN for the highlighted unit cell are illustrated in Fig. 1. Although the smallest allowed TN unit cell for achieving a fully translation invariant square-kagome lat-

tice is  $2 \times 2$ , we conducted our TN simulations using a  $4 \times 4$  unit cell (equivalent to 24 sites on the original square-kagome lattice). This choice was made to ensure detection of all potential phases characterized by nontrivial patterns of spin-spin correlations within the unit cell.

The maximum dimension of virtual bonds achievable within our available computational resources is  $D_{\max} = 12$ . Furthermore, we set the CTMRG boundary dimension to  $\chi = D^2$ . For bond dimensions  $D \geq 8$ , we fix  $\chi = 64$  due to resource constraints. Nevertheless, we observed that this choice sufficed to obtain converged expectation values for various bond dimensions. Furthermore, we used imaginary time evolution during the simple update, initiating with  $\delta\tau = 10^{-1}$  and progressively reducing it to  $10^{-3}$  while allowing a maximum of 3000 iterations for each  $\delta\tau$ . Additionally, we ensured algorithm convergence by monitoring both the energy and singular values obtained during the simple update, terminating the process once a threshold of  $10^{-16}$  was reached.

*Quantum Phase Diagram.* Using our tailored iPEPS algorithm, we simulated the ground state of the model (1) in the parameter range  $0 \leq J/J_1 \leq 2.0$ , for different bond dimensions  $D$ . In order to characterize the phases and phase transitions of the model, we calculate the variational expectation values of different operators ranging from energy to local magnetization and spin-spin correlations. Based on a careful analysis of the evolution of these quantities and their derivatives, together with the bond entanglement entropy, we identify *six* distinct phases in the thermodynamic limit. The quantum phase diagram is shown in Fig. 2 and the iPEPS results supporting the characterization of the underlying phases and phase boundaries are presented in Fig. 3 for the largest bond dimension  $D = 12$ .

The phase boundaries between different nonmagnetic phases are most accurately detected from an assessment of the bond entanglement entropy,  $S_{VN} = \sum_i \lambda_i^2 \log \lambda_i^2$ , where  $\lambda_i$ 's are the singular values obtained from the simple update of PEPS [see Fig. 3(a)]. On the other hand, the phase transitions out of the non-magnetic phases are distinguished from abrupt changes in the average spin-spin correlations [see Fig. 3(b)] as well as the total magnetization and its individual components [see Figs. 3(c) and (d)]. In regions where changes in physical observables were continuous and smooth, we identified the transition points by computing the derivatives from the spline of the observable curve. As shown in Fig. 3(a), in total we observe five transition points separating six phases with distinct patterns of symmetry breaking.

The competition between the  $J$  and  $J_1$  couplings gives rise to broadly two distinct regions in the phase diagram: (i)  $0 \leq J/J_1 \leq 1.62$ : which is nonmagnetic composed of an ensemble of VBCs with different symmetries emerging as the ground state of the system and (ii)  $J/J_1 > 1.62$ : which hosts a ferrimagnetically ordered ground state. In order to characterize the nature of these phases, we compute the local magnetization and spin-spin correlations on individual sites and bonds of the lattice, respectively. Within each region, the pattern of strong and weak bonds in real-space as inferred via equal-time isotropic spin-spin correlations in the ground states is illustrated in Fig. 2. Each phase is uniquely characterized

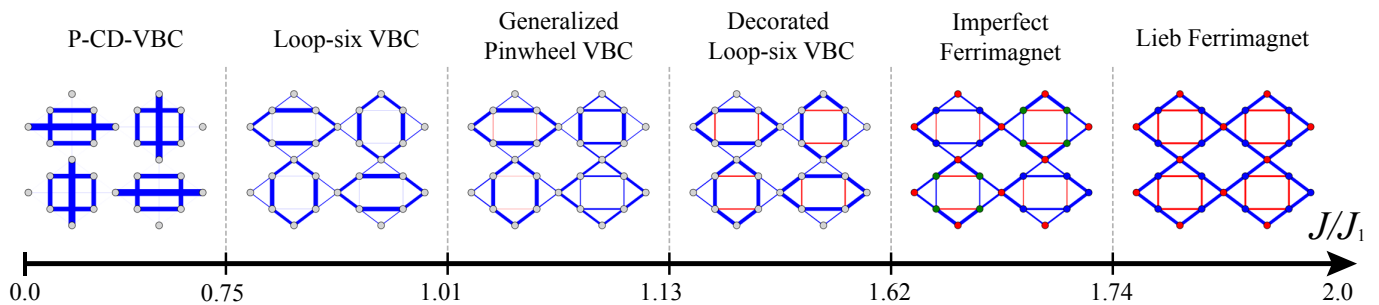


FIG. 2. Quantum phase diagram of the  $S = 1/2$  antiferromagnetic Heisenberg model (1) on the square-kagome lattice obtained using iPEPS up to bond dimension  $D = 12$ . The thickness of the bonds corresponds to the magnitude of the equal-time isotropic spin-spin correlations  $\langle \hat{S}_i \cdot \hat{S}_j \rangle$ . Additionally, the blue (red) bonds represent antiferromagnetic (ferromagnetic) correlations. In the ferrimagnetic phases, the red sites corresponds to a positive total on-site magnetization value, while the blue, and green sites correspond to negative magnetization, with a different strength.

by a distinct pattern of bond correlations or magnetic ordering, as measured on the converged ground state wave function. It is crucial to emphasize that the convergence of the wave function has been thoroughly examined through various measures within the algorithm. As exemplified in Fig. 4, the ground state energy per-site,  $\varepsilon_0$ , for selected points within each region of the phase diagram exhibits excellent convergence with respect to the inverse bond dimension.

We now elaborate on the nature of each of these phases. At  $J/J_1 = 0$ , we have isolated squares with antiferromagnetically interacting spins. Thus, the ground state of the system is plaquette ordered with the four spins forming isolated tetramers with total spin zero. In the limit  $J/J_1 \rightarrow 0$ , we find that the spins at the triangular apex sites are not free but rather form long-range dimers in a checkerboard arrangement [see Fig. 2]. This phase, with long-range singlet formation triggered by a nonzero  $J$  coupling, was predicted within a perturbative treatment of the model [34], and referred to as plaquette crossed-dimer VBC (P-CD-VBC). The P-CD-VBC state is found to be stable till  $J/J_1 \lesssim 0.75$  when it transitions to a loop-six VBC [35]. The location of this transition at  $J/J_1 \sim 0.75$  is consistent with the change in symmetries observed in the ED spectra [34]. In the loop-six VBC [35], which is stabilized due to strong resonances over longer-length loops amplified by the dressing of virtual singlets on top of the nearest-neighbor basis, we find that the bonds with strong antiferromagnetic correlation form closed hexagonal loops in an alternating horizontal and vertical checkerboard pattern. The loop-six VBC is stable over a broad parameter range  $0.75 \leq J/J_1 \leq 1.01$  encompassing the isotropic point  $J/J_1 = 1$ , where previous studies based on quantum dimer models [35] and tensor networks [36] have presented evidence for its ground state candidature. Interestingly, at  $J/J_1 \sim 1$ , in the ED spectra, one notices a change in symmetries of the low excited states, and indeed for  $J/J_1 \geq 1.01$ , our iPEPS calculations find the appearance of a generalized version of the conventional pinwheel VBC [34] which was analyzed as a competing ground state at the isotropic point in earlier VMC [46] and tensor network studies [36]. This generalized pinwheel state has broken reflection symmetries akin to the conventional pinwheel VBC but lacks the  $C_4$  rotation

symmetry which gets lowered to  $C_2$  [see Fig. 2]. This symmetry breaking and the corresponding increase in the number of variational parameters is responsible for its energetic stabilization till  $J/J_1 \leq 1.13$ . Finally, the last phase of the VBC family in the phase diagram is a decorated version of the loop-six VBC and emerges within the range  $1.13 \leq J/J_1 \leq 1.62$ . This state differs from the conventional loop-six VBC state by the appearance of additional parallel alternating horizontal and vertical ferromagnetic correlations on the edges of the squares. These additional correlations can be ascribed as signatures of the incipient ferrimagnetic order that is proximate in the phase diagram, and to which this phase transitions into at  $J/J_1 \sim 1.62$ . Again, this interval of the decorated loop-six VBC approximately coincides with a clearly identifiable distinct region in the ED spectra. In summary, our results show that the quantum phase diagram hosts four types of VBC states in the region  $0 \leq J/J_1 \leq 1.62$ , which are distinguished by distinctive patterns of strong and weak spin-spin correlation of the links of the squares and triangles of the square-kagome lattice.

Next, by increasing  $J/J_1$  beyond 1.62, we enter the second regime of the phase diagram that is spanned by magnetically ordered ground states with a ferrimagnetic spin arrangements on the square and triangular sublattices. It is around  $J/J_1 \sim 1.6$  that one observes a level crossing of states with two different symmetries, which could potentially be linked to this phase transition. In the first phase, which occupies  $1.62 \leq J/J_1 \leq 1.74$ , the spins on the squares are anti-aligned with those of triangles. However, different square sublattices,  $A$  and  $B$ , exhibit different magnitudes for both the  $m_x$  and  $m_z$  components of magnetization [see Fig. 3(d)]. We call this phase an imperfect ferrimagnet due to difference in magnitude of the local magnetization of the square sublattices. However, by increasing the strength of the exchange couplings on triangles we approach the classical limit and transition to a perfect ferrimagnetic state for  $J/J_1 \geq 1.74$ , wherein all spins on squares point in the same direction and with the same magnitude, while they are antiparallel to spins on triangles. This sequence of phases is consistent with a previous exact-diagonalization (ED) study [32, 47]. It is important to note that the shift of the transition to a ferrimagnetic phase to

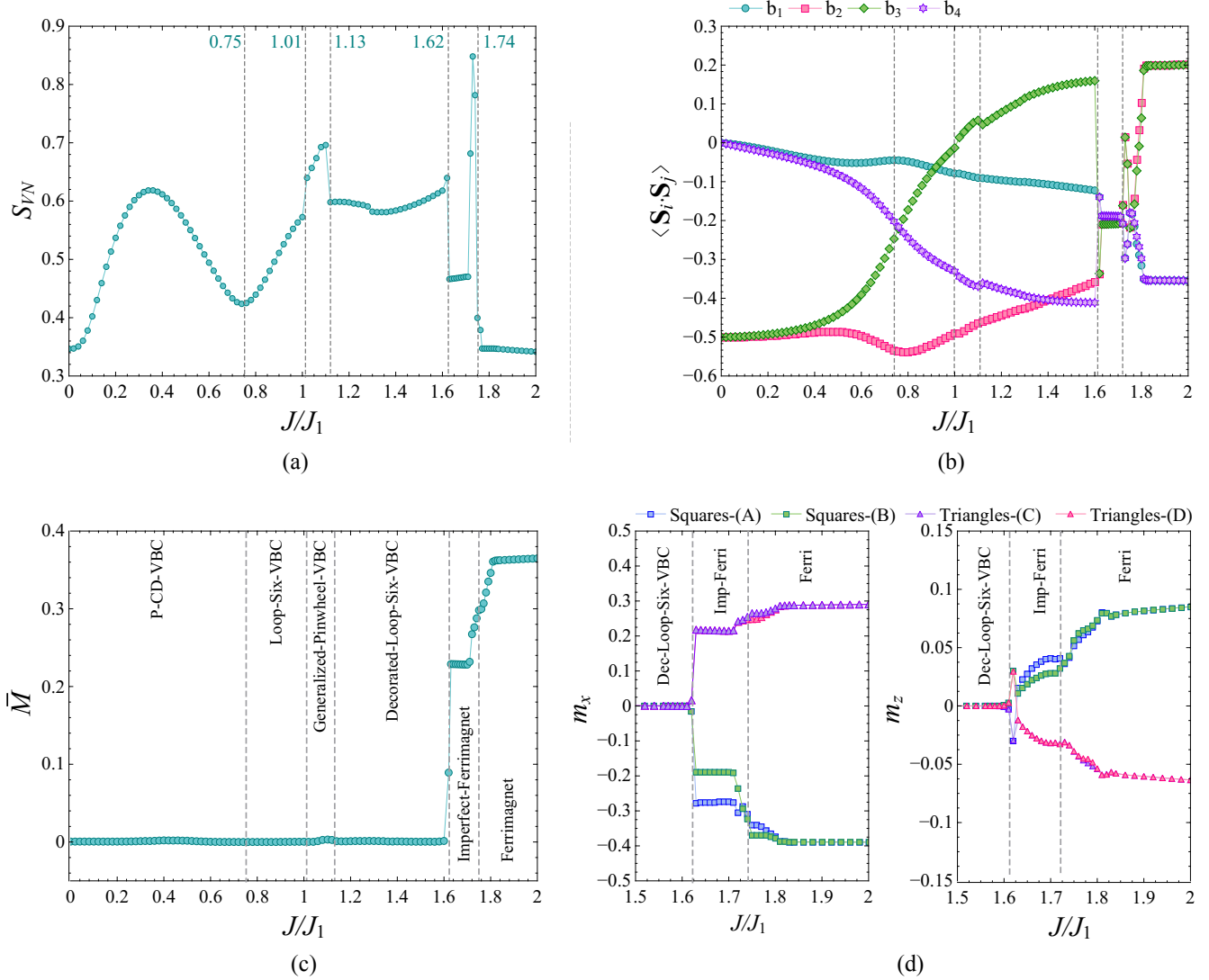


FIG. 3. (a) The bond entanglement entropy, computed from singular value bond matrices of the iPEPS simple update. Vertical dashed lines distinguish the phase boundaries separating distinct phases in the phase diagram. (b) The equal-time isotropic spin-spin correlation  $\langle \hat{S}_i \cdot \hat{S}_j \rangle$ , for the four bonds [see Fig. 1(a) for the link labels] connected to the top-left sites of square  $A$  in Fig. 1(a). (c) Average total magnetization,  $\bar{M} = (1/N) \sum_i M_i$ , with  $M_i = \sqrt{(m_i^x)^2 + (m_i^y)^2 + (m_i^z)^2}$  calculated across all lattice sites. (d) A zoom-in of the average magnetization components,  $m_x$  and  $m_z$ , on the square and triangular sublattices of the unit cell [see Fig. 1(a) for the labeling convention]. All the results in the plot correspond to  $D = 12$  bond dimension.

smaller values compared to its classical value of  $J/J_1 = 2$  is due to the order-by-disorder mechanism which stabilizes the collinear up-up-down state at smaller values of  $J/J_1$ .

This phase is an example of the so-called Lieb Ferrimagnet [48] on the square-kagome lattice, which is an up-up-down state, i.e., the spins on the square and triangular sites are antiparallel, resulting in a net magnetization  $M = 1/3$ . Our iPEPS results further demonstrate that the total spin in the ferrimagnetic ground state is  $S_{\text{tot}} = 3.992$ , in agreement with the theoretical prediction  $S_{\text{tot}} = \frac{|N_T - N_S|}{2} = 4$ , where  $N_T = 8$  and  $N_S = 16$ , respectively, are the number of sites in the triangular and square sublattices of the 24-site unit cell depicted in Fig. 1. This finding reflects the intrinsic sublattice imbalance of the square-kagome lattice. Moreover, our nu-

merical results reveal that the total spin adheres to the condition  $0 < S_{\text{tot}} < \frac{1}{3} M_{\text{sat}}$ , where  $M_{\text{sat}} = 12$  is the saturated magnetization of the unit cell at the 24 site. The observed ferrimagnetic state underscores the consistency of our simulations with the Lieb ferrimagnetic framework and further validates the robustness of our TN simulations for capturing the intricate quantum and classical properties of the ferrimagnetic phases.

*Conclusions.* Using large-scale tensor network calculations based on the infinite projected entangled-pair state algorithm, we present the ground state phase diagram of the  $S = 1/2$  Heisenberg model on the square-kagome lattice with two symmetry-inequivalent nearest-neighbor antiferromagnetic couplings. Within the accuracy of our approach, we

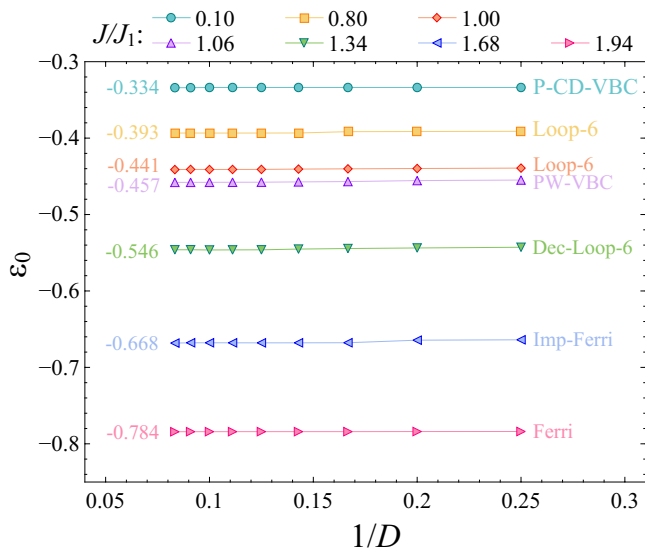


FIG. 4. Scaling of the energy per site versus the inverse bond dimension  $1/D$  for selected points within each phase. The evident convergence of TN simulations with respect to bond dimension is observed across all phases. The numerical values on the left side of each curve correspond to ground state energy per site,  $\varepsilon_0$ , for  $D = 12$  at the selected point within each phase.

find that the model has a nonmagnetic singlet ground state for  $0 \leq J/J_1 \leq 1.62$  and a ferrimagnetic ground state for  $J/J_1 \geq 1.62$ , in agreement with the findings in Ref. [47]. The nonmagnetic region hosts four distinct VBC orders with different patterns of spin-spin correlations. These VBCs can also be viewed as instabilities of parent gapless spin liquids [49] such as those classified in Ref. [46]. It would be important to identify the parent spin liquid and to identify the mechanism of dimerization, i.e., fermion bilinear instability or condensation of singlet monopoles [50, 51]. This could be assessed within a variational Monte Carlo approach which has been

successful in ascertaining the nature of dimer instabilities of gapless spin liquids on the kagome lattice [52–54].

As a natural continuation for future studies, it would be interesting to investigate the thermodynamics of this model [55–59] within a tensor network approach [60]. It was argued in Ref. [34] that the inclusion of a magnetic field would induce the elusive spin-nematic phases, whose detection within a TN framework would constitute an important step. In search of QSL behavior, it would be worthwhile to assess the effect of quantum fluctuations on the classical phase diagram of the nearest-neighbor  $J_1$ - $J_2$ - $J_3$  model which has extended classical spin liquid and Néel ordered phases [61, 62]. In similar vein, the classical noncoplanar orders triggered by long-range Heisenberg couplings [61] could potentially melt under strong quantum fluctuations for  $S = 1/2$  giving rise to chiral spin liquids, which would be worth investigating within a TN framework.

*Acknowledgements.* We thank Ioannis Rousochatzakis and Arnaud Ralko for helpful discussions. S.S.J. acknowledges support from Institute for Advanced Studies in Basic Sciences (IASBS). S.S.J. thanks IIT Madras for a Visiting Faculty Fellow position during which this work was completed. The work of Y.I. was performed in part at the Aspen Center for Physics, which is supported by National Science Foundation Grant No. PHY-2210452 and a grant from the Simons Foundation (1161654, Troyer). This research was supported in part by grant NSF PHY-2309135 to the Kavli Institute for Theoretical Physics (KITP). Y.I. acknowledges support from the ICTP through the Associates Programme, from the Simons Foundation through Grant No. 284558FY19, IIT Madras through the Institute of Eminence (IoE) program for establishing QuCenDiEM (Project No. SP22231244CPETWOQCDHOC), and the International Centre for Theoretical Sciences (ICTS), Bengaluru during a visit for participating in the program: Kagome off-scale (ICTS/KAGOFF2024/08). Y. I. acknowledges the use of the computing resources at HPCE, IIT Madras.

- 
- [1] L. Savary and L. Balents, Quantum spin liquids: a review, *Rep. Prog. Phys.* **80**, 016502 (2016).
- [2] L. Balents, Spin liquids in frustrated magnets, *Nature (London)* **464**, 199 (2010).
- [3] P. Anderson, Resonating valence bonds: A new kind of insulator?, *Mater. Res. Bull.* **8**, 153 (1973).
- [4] R. Moessner and S. L. Sondhi, Resonating Valence Bond Phase in the Triangular Lattice Quantum Dimer Model, *Phys. Rev. Lett.* **86**, 1881 (2001).
- [5] J. T. Chalker, P. C. W. Holdsworth, and E. F. Shender, Hidden order in a frustrated system: Properties of the Heisenberg Kagomé antiferromagnet, *Phys. Rev. Lett.* **68**, 855 (1992).
- [6] D. A. Huse and A. D. Rutenberg, Classical antiferromagnets on the Kagomé lattice, *Phys. Rev. B* **45**, 7536 (1992).
- [7] J. N. Reimers and A. J. Berlinsky, Order by disorder in the classical Heisenberg kagomé antiferromagnet, *Phys. Rev. B* **48**, 9539 (1993).
- [8] J. Richter, J. Schulenburg, P. Tomczak, and D. Schmalfuß, The Heisenberg antiferromagnet on the square-kagomé lattice, *Condens. Matter Phys.* **12**, 507 (2009).
- [9] J. B. Marston and C. Zeng, Spin-Peierls and spin-liquid phases of Kagomé quantum antiferromagnets, *J. Appl. Phys.* **69**, 5962 (1991).
- [10] F. Mila, Low-Energy Sector of the  $S = 1/2$  Kagome Antiferromagnet, *Phys. Rev. Lett.* **81**, 2356 (1998).
- [11] M. B. Hastings, Dirac structure, RVB, and Goldstone modes in the kagomé antiferromagnet, *Phys. Rev. B* **63**, 014413 (2000).
- [12] P. Nikolic and T. Senthil, Physics of low-energy singlet states of the Kagome lattice quantum Heisenberg antiferromagnet, *Phys. Rev. B* **68**, 214415 (2003).
- [13] R. R. P. Singh and D. A. Huse, Ground state of the spin-1/2 kagome-lattice Heisenberg antiferromagnet, *Phys. Rev. B* **76**, 180407 (2007).
- [14] S. Yan, D. A. Huse, and S. R. White, Spin-Liquid Ground State of the  $S = 1/2$  Kagome Heisenberg Antiferromagnet, *Science* **332**, 1173 (2011).
- [15] S. Depenbrock, I. P. McCulloch, and U. Schollwöck, Nature of the Spin-Liquid Ground State of the  $S = 1/2$  Heisenberg

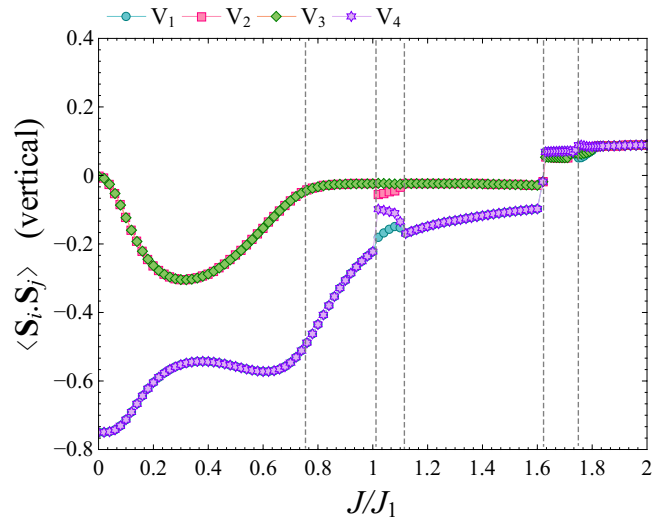
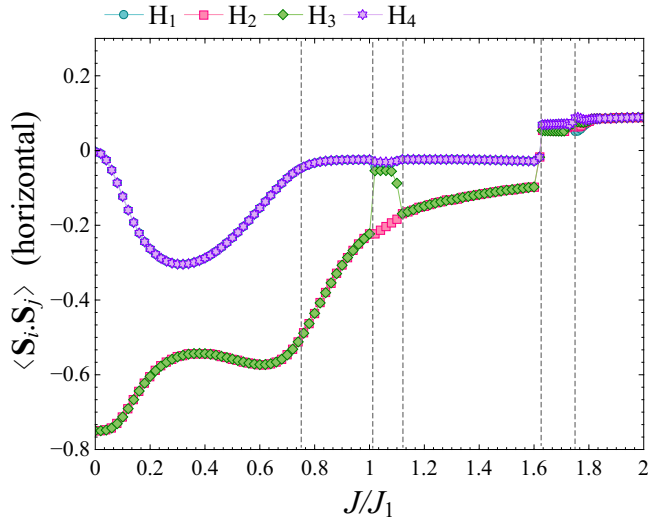


FIG. 5. The crossed-dimer spin-spin correlation on the horizontal and vertical diamonds of the square-kagome lattice. The  $H_i$  and  $V_i$  links have been distinguished in Fig. 6.

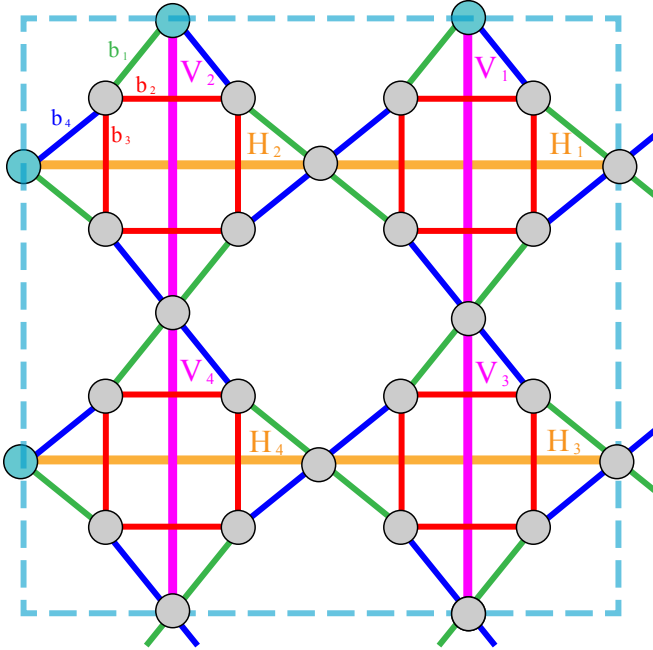


FIG. 6. (a) The 24-site unit cell of the square-kagome lattice with crossed-dimer links. The  $(H_1, \dots, H_4)$  horizontal links and  $(V_1, \dots, V_4)$  vertical links were used in calculation of the crossed-dimer correlation in Fig. 5. Additionally, the links  $(b_1, \dots, b_4)$  correspond to the bonds for which the spin-spin correlation have been shown in Fig. 3(b).

Model on the Kagome Lattice, *Phys. Rev. Lett.* **109**, 067201 (2012).

- [16] P. Khuntia, M. Velazquez, Q. Barthélemy, F. Bert, E. Kermarrec, A. Legros, B. Bernu, L. Messio, A. Zorko, and P. Mendels, Gapless ground state in the archetypal quantum kagome antiferromagnet  $\text{ZnCu}_3(\text{OH})_6\text{Cl}_2$ , *Nat. Phys.* **16**, 469 (2020).
- [17] Y. Ran, M. Hermele, P. A. Lee, and X.-G. Wen, Projected-Wave-Function Study of the Spin-1/2 Heisenberg Model on the

Kagomé Lattice, *Phys. Rev. Lett.* **98**, 117205 (2007).

- [18] Y. Iqbal, F. Becca, S. Sorella, and D. Poilblanc, Gapless spin-liquid phase in the kagome spin- $\frac{1}{2}$  Heisenberg antiferromagnet, *Phys. Rev. B* **87**, 060405 (2013).
- [19] Y. Iqbal, D. Poilblanc, and F. Becca, Vanishing spin gap in a competing spin-liquid phase in the kagome Heisenberg antiferromagnet, *Phys. Rev. B* **89**, 020407 (2014).
- [20] Y.-C. He, M. P. Zaletel, M. Oshikawa, and F. Pollmann, Signatures of Dirac Cones in a DMRG Study of the Kagome Heisenberg Model, *Phys. Rev. X* **7**, 031020 (2017).
- [21] H. J. Liao, Z. Y. Xie, J. Chen, Z. Y. Liu, H. D. Xie, R. Z. Huang, B. Normand, and T. Xiang, Gapless Spin-Liquid Ground State in the  $S = 1/2$  Kagome Antiferromagnet, *Phys. Rev. Lett.* **118**, 137202 (2017).
- [22] R. Siddharthan and A. Georges, Square kagome quantum antiferromagnet and the eight-vertex model, *Phys. Rev. B* **65**, 014417 (2001).
- [23] M. Fujihala, K. Morita, R. Mole, S. Mitsuda, T. Tohyama, S.-i. Yano, D. Yu, S. Sota, T. Kuwai, A. Koda, H. Okabe, H. Lee, S. Itoh, T. Hawai, T. Masuda, H. Sagayama, A. Matsuo, K. Kindo, S. Ohira-Kawamura, and K. Nakajima, Gapless spin liquid in a square-kagome lattice antiferromagnet, *Nat. Commun.* **11**, 3429 (2020).
- [24] T. Goto, M. Fujihala, and S. Mitsuda,  $^{27}\text{Al}$ -NMR study on a square-kagome lattice antiferromagnet, *Interactions* **245**, 40 (2024).
- [25] M. Markina, P. Berdonosov, T. Vasilchikova, K. Zakharov, A. Murtazoev, V. Dolgikh, A. Moskin, V. Glazkov, A. Smirnov, and A. Vasiliev, Static and resonant properties of decorated square kagomé lattice  $\text{KCu}_7(\text{TeO}_4)(\text{SO}_4)_5\text{Cl}$ , *Mater. Chem. Phys.* **319**, 129348 (2024).
- [26] O. V. Yakubovich, L. V. Shvanskaya, G. V. Kiriukhina, A. S. Volkov, O. V. Dimitrova, and A. N. Vasiliev, Hydrothermal Synthesis and a Composite Crystal Structure of  $\text{Na}_6\text{Cu}_7\text{BiO}_4(\text{PO}_4)_4[\text{Cl}(\text{OH})_3]$  as a Candidate for Quantum Spin Liquid, *Inorg. Chem.* **60**, 11450 (2021).
- [27] B. Liu, Z. Zeng, A. Xu, Y. Sun, O. Yakubovich, L. Shvanskaya, S. Li, and A. Vasiliev, Low-temperature specific-heat studies on two square-kagome antiferromagnets, *Phys. Rev. B* **105**, 155153 (2022).

- [28] A. F. Murtazoev, K. A. Lyssenko, M. M. Markina, V. A. Dolgikh, A. N. Vasiliev, and P. S. Berdonosov, New Nabokoite-like Phases  $ACu_7TeO_4(SO_4)_5Cl$  ( $A=Na, K, Rb, Cs$ ) with Decorated and Distorted Square Kagome Lattices, *Chem. Phys. Chem.* **24**, e202300111 (2023).
- [29] Y. Rebrov, V. Glazkov, A. Murtazoev, V. Dolgikh, and P. Berdonosov, High-frequency dielectric anomalies in a highly frustrated square kagomé lattice nabokoite family compounds  $ACu_7TeO_4(SO_4)_5Cl$  ( $A=Na, K, Rb, Cs$ ), *J. Magn. Magn. Mater.* **592**, 171786 (2024).
- [30] N. Niggemann, N. Astrakhantsev, A. Ralko, F. Ferrari, A. Maity, T. Müller, J. Richter, R. Thomale, T. Neupert, J. Reuther, Y. Iqbal, and H. O. Jeschke, Quantum paramagnetism in the decorated square-kagome antiferromagnet  $Na_6Cu_7BiO_4(PO_4)_4Cl_3$ , *Phys. Rev. B* **108**, L241117 (2023).
- [31] M. G. Gonzalez, Y. Iqbal, J. Reuther, and H. O. Jeschke, Field-induced spin liquid in the decorated square-kagome antiferromagnet nabokoite  $KCu_7TeO_4(SO_4)_5Cl$  (2024), arXiv:2410.10385 [cond-mat.str-el].
- [32] K. Morita and T. Tohyama, Magnetic phase diagrams and magnetization plateaus of the spin-1/2 antiferromagnetic Heisenberg model on a square-Kagome lattice with three nonequivalent exchange interactions, *J. Phys. Soc. Jpn.* **87**, 043704 (2018).
- [33] T. Lukan, L. D. C. Jaubert, and A. Ralko, Topological nematic spin liquid on the square Kagome lattice, *Phys. Rev. Research* **1**, 033147 (2019).
- [34] I. Rousochatzakis, R. Moessner, and J. van den Brink, Frustrated magnetism and resonating valence bond physics in two-dimensional kagome-like magnets, *Phys. Rev. B* **88**, 195109 (2013).
- [35] A. Ralko and I. Rousochatzakis, Resonating-valence-bond physics is not always governed by the shortest tunneling loops, *Phys. Rev. Lett.* **115**, 167202 (2015).
- [36] P. Schmoll, A. Kshetrimayum, J. Naumann, J. Eisert, and Y. Iqbal, Tensor network study of the spin- $\frac{1}{2}$  Heisenberg antiferromagnet on the shuriken lattice, *Phys. Rev. B* **107**, 064406 (2023).
- [37] R. Orús, A practical introduction to tensor networks: Matrix product states and projected entangled pair states, *Ann. Phys. (N. Y.)* **349**, 117 (2014).
- [38] R. Orús, Advances on tensor network theory: symmetries, fermions, entanglement, and holography, *Eur. Phys. J. B* **87**, 280 (2014).
- [39] F. Verstraete, V. Murg, and J. Cirac, Matrix product states, projected entangled pair states, and variational renormalization group methods for quantum spin systems, *Adv. Phys.* **57**, 143 (2008).
- [40] R. Orús and G. Vidal, Simulation of two-dimensional quantum systems on an infinite lattice revisited: Corner transfer matrix for tensor contraction, *Phys. Rev. B* **80**, 094403 (2009).
- [41] H. N. Phien, J. A. Bengua, H. D. Tuan, P. Corboz, and R. Orús, Infinite projected entangled pair states algorithm improved: Fast full update and gauge fixing, *Phys. Rev. B* **92**, 035142 (2015).
- [42] S. S. Jahromi, R. Orús, M. Kargarian, and A. Langari, Infinite projected entangled-pair state algorithm for ruby and triangle-honeycomb lattices, *Phys. Rev. B* **97**, 115161 (2018).
- [43] H. C. Jiang, Z. Y. Weng, and T. Xiang, Accurate Determination of Tensor Network State of Quantum Lattice Models in Two Dimensions, *Phys. Rev. Lett.* **101**, 090603 (2008).
- [44] T. Nishino and K. Okunishi, Corner Transfer Matrix Renormalization Group Method, *J. Phys. Soc. Jpn.* **65**, 891 (1996).
- [45] S. S. Jahromi, R. Orús, D. Poilblanc, and F. Mila, Spin- $\frac{1}{2}$  kagome Heisenberg antiferromagnet with strong breathing anisotropy, *SciPost Phys.* **9**, 092 (2020).
- [46] N. Astrakhantsev, F. Ferrari, N. Niggemann, T. Müller, A. Chauhan, A. Kshetrimayum, P. Ghosh, N. Regnault, R. Thomale, J. Reuther, T. Neupert, and Y. Iqbal, Pinwheel valence bond crystal ground state of the spin- $\frac{1}{2}$  Heisenberg antiferromagnet on the shuriken lattice, *Phys. Rev. B* **104**, L220408 (2021).
- [47] J. Richter and J. Schnack, Magnetism of the  $S = \frac{1}{2}J_1 - J_2$  square-kagome lattice antiferromagnet, *Phys. Rev. B* **107**, 245115 (2023).
- [48] E. H. Lieb, Two theorems on the Hubbard model, *Phys. Rev. Lett.* **62**, 1201 (1989).
- [49] X.-Y. Song, C. Wang, A. Vishwanath, and Y.-C. He, Unifying description of competing orders in two-dimensional quantum magnets, *Nat. Commun.* **10**, 4254 (2019).
- [50] S. Budaraju, Y. Iqbal, F. Becca, and D. Poilblanc, Piercing the Dirac spin liquid: From a single monopole to chiral states, *Phys. Rev. B* **108**, L201116 (2023).
- [51] S. Budaraju, A. Parola, Y. Iqbal, F. Becca, and D. Poilblanc, Monopole excitations in the  $U(1)$  Dirac spin liquid on the triangular lattice (2024), arXiv:2410.18747 [cond-mat.str-el].
- [52] Y. Iqbal, F. Becca, and D. Poilblanc, Valence-bond crystal in the extended kagome spin- $\frac{1}{2}$  quantum Heisenberg antiferromagnet: A variational Monte Carlo approach, *Phys. Rev. B* **83**, 100404 (2011).
- [53] Y. Iqbal, F. Becca, and D. Poilblanc, Valence-bond crystals in the kagomé spin-1/2 Heisenberg antiferromagnet: a symmetry classification and projected wave function study, *New J. Phys.* **14**, 115031 (2012).
- [54] Y. Iqbal, D. Poilblanc, R. Thomale, and F. Becca, Persistence of the gapless spin liquid in the breathing kagome Heisenberg antiferromagnet, *Phys. Rev. B* **97**, 115127 (2018).
- [55] P. Tomczak and J. Richter, Specific heat of the spin- Heisenberg antiferromagnet on Squagome lattice, *J. Phys. A* **36**, 5399 (2003).
- [56] H. Nakano and T. Sakai, The two-dimensional  $S=1/2$  Heisenberg antiferromagnet on the Shuriken lattice – a lattice composed of vertex-sharing triangles, *J. Phys. Soc. Jpn.* **82**, 083709 (2013).
- [57] O. Derzhko, J. Richter, O. Krupnitska, and T. Krokhnalskii, The square-kagome quantum Heisenberg antiferromagnet at high magnetic fields: The localized-magnon paradigm and beyond, *Low Temp. Phys.* **40**, 513 (2014).
- [58] Y. Hasegawa, H. Nakano, and T. Sakai, Metamagnetic jump in the spin- $\frac{1}{2}$  antiferromagnetic Heisenberg model on the square kagome lattice, *Phys. Rev. B* **98**, 014404 (2018).
- [59] J. Richter, O. Derzhko, and J. Schnack, Thermodynamics of the spin-half square kagome lattice antiferromagnet, *Phys. Rev. B* **105**, 144427 (2022).
- [60] P. Schmoll, H. O. Jeschke, and Y. Iqbal, Tensor network analysis of the maple-leaf antiferromagnet spangolite (2024), arXiv:2404.14905 [cond-mat.str-el].
- [61] M. Gembé, H.-J. Schmidt, C. Hickey, J. Richter, Y. Iqbal, and S. Trebst, Noncoplanar magnetic order in classical square-kagome antiferromagnets, *Phys. Rev. Res.* **5**, 043204 (2023).
- [62] K. B. Yogendra, S. Karmakar, and T. Das, Symmetry, superposition, and fragmentation in classical spin liquids: A general framework and applications to square kagome magnets, *Phys. Rev. B* **110**, L060401 (2024).